Effects of size and arrangement of virtual transducer on photoacoustic tomography*

Wang Shao-Hua(王少华), Tao Chao(陶 超)†, and Liu Xiao-Jun(刘晓峻)‡

Key Laboratory of Modern Acoustics, Nanjing University, Nanjing 210093, *China*

(Received 8 October 2012; revised manuscript received 19 November 2012)

In this paper, we investigate the effects of the relative size and arrangement of a virtual transducer on the image quality in limited-view photoacoustic tomography. A virtual transducer refers to the acoustic scatterers used to reflect photoacoustic waves and improve the images reconstructed from incomplete PA signal. Size and spatial arrangement determine the performance of the virtual transducer. In this study, the scatterers utilized as virtual transducers are arranged in different manners, such as on a straight line or on an arc line. We find that virtual transducers with a big distributing angle can provide more significant image improvement than with a small distributing angle, which is similar to the true transducers. We also change the size of virtual transducer and study its influence on image quality. It is found that the bigger scatterers provide better images than the smaller ones. Especially, when the size of scatterers is reduced to the wavelength of photoacoustic wave, the image quality observably decreases, owing to the strong diffraction effect. Thus, it is suggested that the size of the acoustical scatterers should be much larger than the photoacoustic wavelength. The simulations are conducted, and the results could be helpful for the application and further study of virtual transducer theory in limited-view photoacoustic tomography.

Keywords: photoacoustic tomography, limited-view, virtual transducer, scattering

PACS: 43.35.Ud, 43.60.Pt **DOI:** 10.1088/1674-1056/22/7/074303

1. Introduction

Photoacoustic tomography (PAT) is a hybrid imaging technology with great promises due to its outstanding performance in high contrast, adequate penetration depth, good resolution in deep tissue, and safety.[1–3] Firstly, compared with the pure ultrasound imaging, where the acoustic impedance is used as an image parameter, PAT imaging uses the optical absorption as an image parameter, and it can provide higher contrast and more functional information about biological tissue. Secondly, PAT provides a better spatial resolution in deep tissue than optical imaging, since the acoustic scattering is much weaker than the optical scattering in soft tissues. Thirdly, the non-ionizing wave (e.g., laser, microwave) employed in PAT is much safer for biological tissues than the ionizing X-ray. Integrating these advantages together, PAT becomes one of the fastest growing fields in the nondestructive testing techniques in biological tissue.[4–6] The applications of PAT have covered many aspects of biomedical imaging such as vascular imaging,[7,8] brain imaging of small animals,[9,10] breast cancer detection,[11,12] the study of oxygen saturation and the concentration of hemoglobin,[13,14] etc.

Theoretically, full-view PAT can provide exact deposition information about optical absorption in the region of interest.[15] It is said that an exact reconstruction solution of the initial source can be derived from the whole photoacoustic signals surrounding the region,[16] where the ultrasound transducer is needed to collect the signals on a closed circle for two-dimensional cases or on a closed sphere for three-dimensional cases. This is full-view PAT. Unfortunately, it could be difficult to obtain the full photoacoustic signals from all orientations in some practical cases, e.g., the scanning angle is always less than 180° for breast image reconstruction.[12] Studies have shown that incomplete data due to the limited-view scanning could weaken the quality of the reconstructed PAT images.[17–19] Many efforts have been made to solve the limited view problem. Xu *et al.*[20] analytically explained the influence of limited-view scanning on the filtered back-projection algorithm. Paltauf *et al.*[21] experimentally investigated limited-view PAT. Tao and Liu[18] proposed an iterative reconstruction algorithm to improve the image quality reconstructed from the incomplete PA data collected within a narrow scanning angle.

Recently, Wu *et al.*[22] utilized backscatterers as virtual transducers to improve the quality of image reconstructed from incomplete PA signal. In this scheme, the diffused waves reflected by the scatterers located in the back of the absorber are gathered to reconstruct a better image. This study showed that the enhanced image can be acquired by taking advantage of the scattered waves in the case of limited-view scanning. It suggested that utilizing the nature scatterers (e.g., bones in

*Project supported by the National Basic Research Program of China (Grant No. 2012CB921504), the National Natural Science Foundation of China (Grant Nos. 11274167, 11274171, and 11074124), and the State Key Laboratory of Acoustics, Chinese Academy of Sciences (Grant No. SKLA201208).

†Corresponding author. E-mail: taochao@nju.edu.cn

‡Corresponding author. E-mail: liuxiaojun@nju.edu.cn

© 2013 Chinese Physical Society and IOP Publishing Ltd

tissues) or artificial ones (e.g., injection of ultrasound contrast agent microbubbles) as virtual transducers can record the backside sound waves.

Since acoustic scatterers play the role of a virtual transducer in this imaging scheme, their configuration and spatial arrangement are two key factors which determine the performance of the image quality. How does the spatial arrangement of the virtual transducers affect the image reconstruction? What is the relationship between the image quality and the scatterer configuration (e.g., the size)? Investigations in these respects are still very inadequate. In this study, we will answer these questions raised in the practical application of virtual transducer method by using the numerical experiments based on finite element method (FEM). In Section 2, the theory of virtual transducer is briefly reviewed and the setup of numerical experiments is introduced. In Section 3, numerical experiments based on FEM are implemented to investigate the influence of configuration and arrangement of acoustic scatterers on image quality. Finally, conclusions are drawn in Section 4.

2. Methods

2.1. Theory of virtual transducer

We introduce the theory of the virtual transducer briefly in this subsection.[22] We consider the scenario presented in Fig. 1. When a pulsed laser with an extremely short width $T_{\rm p}$ irradiates the region of interest (ROI), tissues absorb optical energy and the initial acoustic pressure $p(\boldsymbol{r}_0, t=0)$ is proportional to the optical energy absorption deposition $A(\boldsymbol{r}_0)$. So the initial pressure field can indicate the spatial source generated by optical absorption. The generation and propagation of photoacoustic field $p(\boldsymbol{r}, t)$ is governed by[23]

$$\nabla \cdot \left(\frac{1}{\rho}\nabla p\right) - \frac{1}{\rho c^2}\frac{\partial^2 p(\boldsymbol{r},t)}{\partial t^2} = -p_0(\boldsymbol{r})\frac{\partial \delta(t)}{\partial t}, \qquad (1)$$

where ρ is the density of tissue and c is the speed of sound.

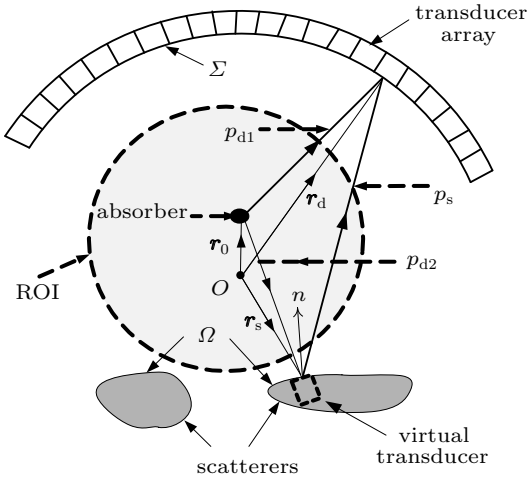


Fig. 1. Scenario of virtual transducer, where Σ and Ω represent the boundaries of the transducer array and the scatterers, respectively.

An ultrasonic transducer array is used to record the PA pressure $p(\boldsymbol{r}_{\rm d}, t)$. Solving Eq. (1), the sound pressure in the time interval $t \in [0, T]$ recorded at position $\boldsymbol{r}_{\rm d}$ can be expressed as

$$p(\boldsymbol{r}_{\rm d}, t) = \int_0^T {\rm d}t_0 \int\int\int_R {\rm d}\boldsymbol{r}_0 q(\boldsymbol{r}_0, t_0) g(\boldsymbol{r}_{\rm d}, t|\boldsymbol{r}_0, t_0), \qquad (2)$$

where $q(\boldsymbol{r}_0, t_0)$ is the acoustic source and $g(\boldsymbol{r}_{\rm d}, t|\boldsymbol{r}_0, t_0)$ represents the Green's function in the scattering tissue. If the wavelength of PA wave is much smaller than the size of the scatterers, the backscattering can be approximated by the mirror reflection and the Green's function can be given as

$$g(\boldsymbol{r}_{\rm d}, t|\boldsymbol{r}_0, t_0) \approx g_1(\boldsymbol{r}_{\rm d}, t|\boldsymbol{r}_0, t_0) + \int\int_\Omega {\rm d}\boldsymbol{r}_{\rm s} g_2(\boldsymbol{r}_{\rm d}, t|\boldsymbol{r}_0, t_0)\boldsymbol{\Theta}(\theta_i, \theta_o) \qquad (3)$$

with

$$g_1(\boldsymbol{r}_{\rm d}, t|\boldsymbol{r}_0, t_0) = \frac{\delta\left(t - t_0 - |\boldsymbol{r}_0 - \boldsymbol{r}_{\rm d}|/c\right)}{4\pi|\boldsymbol{r}_0 - \boldsymbol{r}_{\rm d}|},$$

$$g_2(\boldsymbol{r}_{\rm d}, t|\boldsymbol{r}_0, t_0) = \frac{\delta\left(t - t_0 - |\boldsymbol{r}_0 - \boldsymbol{r}_{\rm s}|/c - |\boldsymbol{r}_{\rm d} - \boldsymbol{r}_{\rm s}|/c\right)}{4\pi(|\boldsymbol{r}_0 - \boldsymbol{r}_{\rm s}| + |\boldsymbol{r}_{\rm d} - \boldsymbol{r}_{\rm s}|)},$$

where $\boldsymbol{\Theta}(\theta_{\rm i}, \theta_{\rm o})$ is the Kronecker delta function, $\theta_{\rm i}$ and $\theta_{\rm o}$ are the incidence and reflection angles, respectively, Ω is the hard boundary of the scatterers, $g_1(\boldsymbol{r}_{\rm d}, t|\boldsymbol{r}_0, t_0)$ is the Green's function in homogeneous tissue, which describes the propagation of the direct wave (e.g., $p_{\rm d1}$ in Fig. 1). The latter term of the equation is the Green's function of the backscatterers, which corresponds to the backscattered wave traveling along the path given by $p_{\rm d2}$ and $p_{\rm s}$ in Fig. 1.

Time reversing $p(\boldsymbol{r}_{\rm d}, t)$ to $p(\boldsymbol{r}_{\rm d}, T-t)$ and retransmitting $p(\boldsymbol{r}_{\rm d}, T-t)$, we have the time reversal (TR) pressure field $p_{\rm TR}(\boldsymbol{r}_0, t)$ in ROI

$$p_{\rm TR}(\boldsymbol{r}_0, t) = \int_0^T {\rm d}t_1 \int\int_\Sigma {\rm d}\boldsymbol{r}_{\rm d} p(\boldsymbol{r}_{\rm d}, T - t_1) g(\boldsymbol{r}_0, t|\boldsymbol{r}_{\rm d}, t_1). \qquad (3)$$

And if the region of interest is closed in the domain of integration Σ, it was proved that $p_{\rm TR}(\boldsymbol{r}_0, t) = p(\boldsymbol{r}_0, T-t)$ and the eventual time reversal pressure field $p_{\rm TR}(\boldsymbol{r}_0, t=T)$ is consistent with the initial pressure $p(\boldsymbol{r}_0, 0)$.[24] Hence, the time reversal pressure can denote the optical energy absorption function $A(\boldsymbol{r}_0)$. However, when the domain Σ cannot enclose ROI, the quality of reconstructed image would be degraded because of the missing data from the unclosed region. However, when backscatters exist, we can substitute Eq. (3) into Eq. (3) and the field $p_{\rm TR}(\boldsymbol{r}_0, t)$ can be rewritten as

$$p_{\rm TR}(\boldsymbol{r}_0, t) = \int_0^{\rm T} {\rm d}t_1 \Big[\int\int_\Sigma {\rm d}\boldsymbol{r}_{\rm d} p_t(\boldsymbol{r}_0, t|\boldsymbol{r}_{\rm d}, t_1) + \int\int_\Omega {\rm d}\boldsymbol{r}_{\rm s} p_{\rm s}(\boldsymbol{r}_0, t|\boldsymbol{r}_{\rm s}, t_1)\Big]. \qquad (4)$$

Then $p_t(\boldsymbol{r}_0, t|\boldsymbol{r}_{\rm d}, t_1) = p(\boldsymbol{r}_{\rm d}, T-t_1) g_1(\boldsymbol{r}_0, t|\boldsymbol{r}_{\rm d}, t_1)$ denotes the re-emitting time reversed direct waves from actual transducers. Whereas, $p_{\rm s}(\boldsymbol{r}_0, t|\boldsymbol{r}_{\rm s}, t_1) = \int\int_\Sigma {\rm d}\boldsymbol{r}_{\rm d} p(\boldsymbol{r}_{\rm d}, T -$

$t_1)g_2(\boldsymbol{r}_0,t|\boldsymbol{r}_\mathrm{d},t_1)\Theta(\theta_\mathrm{i},\theta_\mathrm{o})$ denotes re-emitting time-reversed backscattered waves from backscatterers. Although the back-propagating PA waves (e.g., $p_{\mathrm{d}2}$ in Fig. 1) cannot be directly detected by the transducer array, they could be recorded after being reflected by the virtual transducers. In this case, scatterers [the second term on the right-hand side of Eq. (4)] fulfill a similar function to the transducers [the first term on the right-hand side of Eq. (4)]. Therefore, they are considered as virtual transducers placed at back of ROI in this study and their contribution to TR field is $p_\mathrm{s}(\boldsymbol{r}_0,t|\boldsymbol{r}_\mathrm{s},t_1)$. Since these virtual transducers capture the back-propagating information, backscattered waves can compensate for the direct waves which are not directly detected, and be exploited to produce better images.

2.2. Numerical experiments

The setup of numerical experiment is shown in Fig. 2. The solid circular arc with a radius of 30.0 mm denotes the scanning orbit, where the angle θ quantitatively determines the scanning range of the ultrasound transducer. The black circle denotes the optical absorber. Its diameter is 4.0 mm. The seven gray circles represent the acoustic scatterers. Two kinds of spatial arrangements of scatterers are studied. The first one is shown in Fig. 2(a), where all scatterers are symmetrically distributed with respect to the y axis and equidistantly located on an arc line with a radius $r = 24.0$ mm. Another kind of distribution is shown in Fig. 2(b), where all scatterers are equidistantly located on a straight line $y = 16.0$ mm and the distance l between any two contiguous scatterers is 7.0 mm. The distributing angle α is used to measure the distributing range of the virtual transducers quantitatively as shown in Figs. 2(a) and 2(b).

The optical absorber and the background medium are given with the density $\rho = 1000$ kg/m^3 and the speed of sound $c = 1500$ m/s, which are close to the acoustic properties of soft tissue. The relatively optical absorption is given as $A(\boldsymbol{r}) = 1.0$ inside the absorbers, which represents those tissues with relatively strong optical absorption, such as blood vessels. And the relative optical absorption is set as $A(\boldsymbol{r}) = 0.0$ for the other region. A Gaussian laser pulse is used to excite the photoacoustic signal, which has a central frequency of 1.8 MHz and 3-dB bandwidth of 2.8 MHz. The sound hard boundary condition is imposed on the boundary of the acoustic scatterers (the gray circles) to simulate the strong acoustic scattering. And the photoacoustic signal is recorded with the sampling rate 20 MHz.

In this study, we will manipulate the size and arrangement of the acoustic scatterers and study the influence of these factors on the image quality.

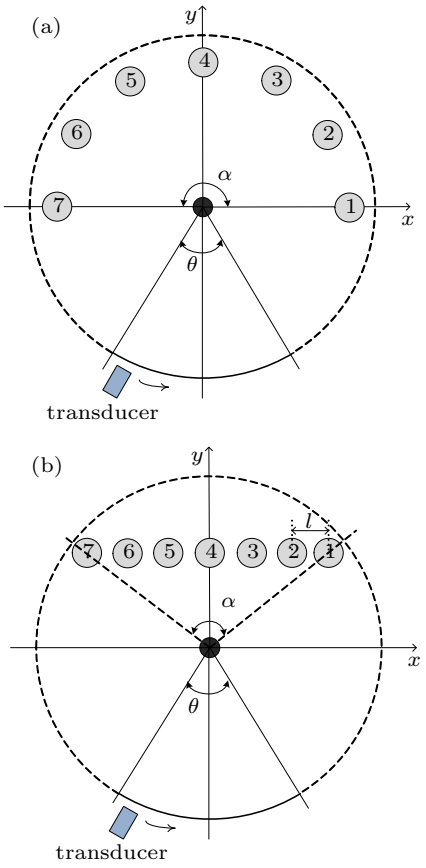


Fig. 2. (color online) Schematic diagram of the numerical experiment setups, showing (a) the scatterers arranged on an arc line and (b) the scatterers posed on a straight line paralleled to the x axis. The angle α describes the distributing range of the acoustic scatterers and the angle θ is the scanning angle of the ultrasound transducers.

3. Results and discussion

Figure 3 visually illustrates the influences of the size and arrangement of the scatterers on the image quality, where all of these images are reconstructed from the limited-view PAT data obtained within the same scanning angle ($\theta = 60^\circ$), but the arrangements and sizes of scatterers are different. All scatterers are posted on an arc line as shown in Fig. 2(a). The three columns from the left to the right correspond to the scatterers with the radii of 1.0 mm, 2.0 mm, and 3.0 mm, respectively. The upper and lower rows correspond to the values of distributing angle α, 180° and 135° respectively. As shown in Fig. 3, both the arrangement and size of the scatterers could influence the image quality. The bigger scatterers [e.g., the scatterers with a radius of 3.0 mm in Figs. 3(c) and 3(f)] provide better images than the smaller scatterers [e.g., the scatterers with a radius of 1.0 mm in Figs. 3(a) and 3(d)]. Also, we can notice that when the scatterers are arranged within a larger region (the upper row, $\alpha = 180^\circ$), the obtained images are better than those when the scatterers are posed within a smaller region (the lower row, $\alpha = 135^\circ$).

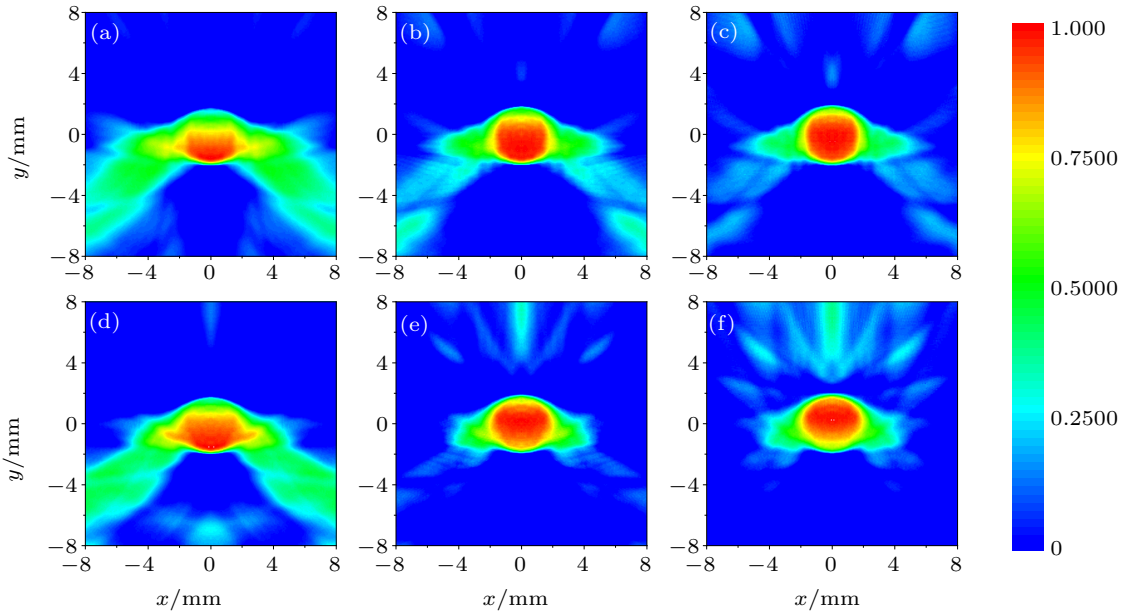


Fig. 3. (color online) Images obtained from incomplete photoacoustic signals by using the virtual transducer method, where photoacoustic signals are detected with the same scanning angle $\theta = 60°$, but the acoustic scatterers (virtual transducers) have different sizes and spatial distributions. The three columns from the left to the right correspond to the radii of the scatterers 1.0 mm, 2.0 mm, and 3.0 mm, respectively. The upper and lower rows correspond to the distributing angles $\alpha = 180°$ and 135°, respectively.

In order to investigate the influences of the arrangement and size of scatterers quantitatively, we use the full width at half-maximum (FWHM) to quantify image quality. We firstly calculate the maximum intensity projection of the reconstructed image on the x axis and determine the positions of the half-maximum. Finally, we obtain the FWHM value of the maximum intensity projection of the reconstructed image. Figure 4 gives the FWHM values obtained with different spatial distributions of the scatterers, where the y axis represents the FWHM value, and the x axis the value of scanning angle θ of the ultrasonic transducer.

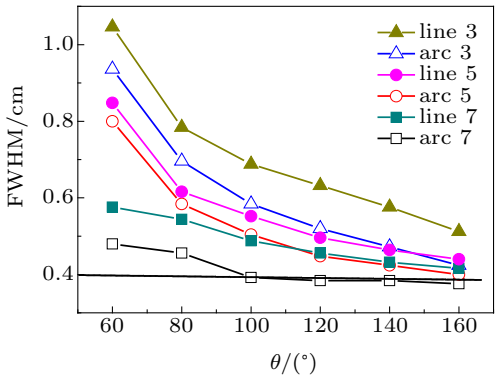


Fig. 4. (color online) FWHM values with the different numbers and arrangements of scatterers. The three kinds of empty symbols are obtained from the scene in Fig. 2(a), where the scatterers are posed on an arc line. The three kinds of solid symbols are obtained from the scene in Fig. 2(b), where the scatterers are posed on a straight line. The dotted line represents the actual diameter of the absorber.

Two kinds of spatial distributions are compared in this figure. One is that the seven scatterers are equally spaced on a line at $y = 16.0$ mm and the interval between any two adjacent scatterers is 7.0 mm as shown in Fig. 2(b). The FWHM results are shown in Fig. 4 with the solid symbols. The other one is the half-circle distribution as shown in Fig. 2(a). The FWHM value is plotted in Fig. 4 with the empty symbols correspondingly. As shown, with the same number of scatterers, the FWHM value obtained from the half-circle distribution is closer to the actual absorber diameter (4.0 mm) than that obtained from the straight distribution, which indicates that the image quality with the half-circle distribution [shown in Fig. 2(a)] is better than that with the straight distribution [shown in Fig. 2(b)].

In order to explain this phenomenon, we reconsider Eq. (4) deduced in the theory part. The equation covers two parts, i.e., the direct waves from the actual transducers (integrating on the boundary Σ) and the backscattered waves from the virtual transducers (integrating on the boundary Ω). We have indicated that the incomplete data would degrade the image quality.[22] The bigger view angle will obtain a bigger integral boundary Σ and the bigger number of scatterers will also obtain a more broad integral boundary Ω. Thus, it is obvious that the more useful information will be obtained in big view angle and so the reconstructed images will be very accurate. When the scatterers are posed on a straight line, these scatterers only capture the backscattering signal within the angle α [see Fig. 2(b)], which is smaller than that picked up by those scatterers posed on a half-circle [see Fig. 2(a)]. In other words, the distributing angle of the virtual transducer of a straight distribution is smaller than that of the half-circle. Therefore, this spatial distribution makes the virtual transducers (scatterers) have a bigger distributing angle α, which will provide a better image quality. The virtual transducer (acoustic scatterer) has

the same properties as the true transducer in this aspect.

In order to examine the above hypothesis, figure. 5 shows the comparison between image qualities when the virtual transducer has different distributing angles, where the seven scatterers are equally spaced on the arc with the angle $\alpha = 90°$, 135°, and 180°, respectively. If the scatterers are distributed on an arc with $\alpha = 90°$, the FWHM value of the obtained image (the solid circles) is much larger than the actual absorber diameter, which means a bad reconstruction. However, for the same scatterers, if they are distributed on big arcs with $\alpha = 135°$ and 180°, the FWHM values (the solid triangles and the squares) decrease and are closer to the actual absorber diameter, which means a good reconstruction. These results clearly manifest that the images become better when the scatterers are arranged within a bigger distributing angle as observed in the above analysis. In addition, it can be noticed that the extremely small distributing angles, e.g., $\alpha = 90°$, will significantly reduce the quality of the reconstructed images. This is because the multiple reflection of PA signal between the close scatterers can degrade the reconstructed image.

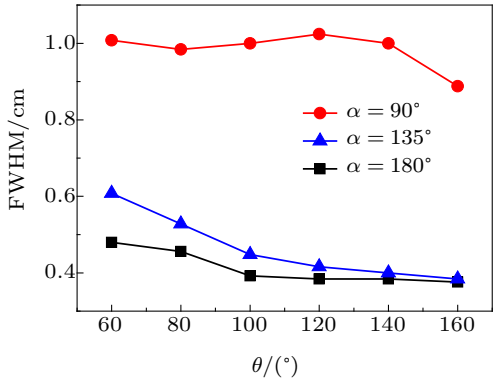


Fig. 5. (color online) FWHM versus scanning angle θ with different distributing angles of the virtual transducers. The lines from the top to the bottom correspond to the distributing angles α of 90°, 135° and 180°, respectively.

The influence of the scatterer size on the quality of image is also investigated. Figure 6 gives the FWHM values of the image obtained from the virtual transducers with various scatterer radii. Seven scatterers are arranged on a half-circle as shown in Fig. 2(a). The control parameter is the radius of the scatterers. For example, the scatter radii are taken to be 1.0 mm, 2.0 mm, or 3.0 mm separately. As shown in Fig. 6, the image obtained by the virtual transducer with the bigger scatterers (3.0 mm) has a smaller FWHM value, which is closer to the actual absorber diameter. Especially, when the radius of the scatterers is only 1.0 mm, the boundary of the image becomes blurred and the distortion is observed clearly as shown in Figs. 3(a) and 3(d). In this situation, the image improvement by the virtual transducer is very limited.

Finally, we discuss the influence of scatterer size on the image quality. In the numerical experiment, the central frequency of the initial Gauss pulse is 1.8 MHz. Its corresponding wavelength is about 0.8 mm in tissue, which is close to the size of scatterers with a radius of 1 mm. However, the theory of virtual transducer [see Eq. (4)] requires that the size of the acoustic scatterers is much larger than the photoacoustic wavelength in order to obtain an effective ultrasound reflection. When the size of the scatterers is comparable to the wavelength of the sound wave, the mirror reflection is weak but the diffraction becomes strong. Especially, the low frequency component of photoacoustic signal cannot be well reflected by the small scatterers. Then, the absence of the lower frequency photoacoustic information should degrade the image quality. Therefore, the bigger scatterers provide the better image quality than the smaller ones.

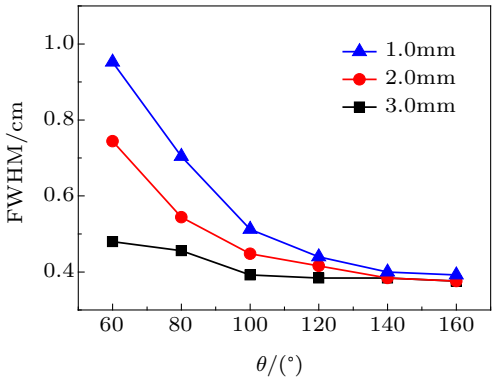


Fig. 6. (color online) FWHM values with the different scatterer radii. The triangle, dot, and square symbols represent the radii of scatterers of 1.0 mm, 2.0 mm, and 3.0 mm, respectively.

4. Conclusions

The influences of the size and spatial arrangement of the virtual transducers on image quality are quantitatively investigated. When the arrangement of the scatterers is posed in a more broad scope, i.e., the virtual transducer (scatterer) has a bigger distributing angle α, the image improvement is remarkable. The virtual transducer has the similar properties to the true transducer in this aspect. However, it is different from a true transducer that the bigger virtual transducers provide better image quality than the smaller ones. Especially, when the size of scatterers is reduced to the wavelength of photoacoustic wave, the image quality is observably degraded, owing to the strong diffraction and the deficiency of the low frequency component. Therefore, the results proposed in this study are helpful for optimizing virtual transducer and carrying forward the application of virtual transducer theory in limited-view photoacoustic tomography.

References

[1] Sun T and Diebold G J 1992 *Nature* **355** 806
[2] Xu M H and Wang L H V 2006 *Rev. Sci. Instrum.* **77** 041101
[3] Kong F, Chen Y C, Lloyd H O, Silverman R H, Kim H H, Cannata J M and Shung K K 2009 *Appl. Phys. Lett.* **94** 033902

[4] Wang X D, Pang Y J, Ku G, Xie X Y, Stoica G and Wang L H V 2003 *Nat. Biotechnol.* **21** 803
[5] Zhang H F, Maslov K, Stoica G and Wang L H V 2006 *Nat. Biotechnol.* **24** 848
[6] Wang L H V and Hu S 2012 *Science* **335** 1458
[7] Oladipupo S S, Hu S, Santeford A C, Yao J J, Kovalski J R, Shohet R V, Maslov K, Wang L V and Arbeit J M 2011 *Blood* **117** 4142
[8] Xiang L Z, Xing D, Gu H M, Yang D W, Yang S H and Zeng L M 2007 *Acta Phys. Sin.* **56** 3911 (in Chinese)
[9] Xu M H, Xu Y and Wang L H V 2003 *IEEE Trans. Biomed. Eng.* **50** 1086
[10] Yang S H and Yin G Z 2009 *Acta Phys. Sin.* **58** 4760 (in Chinese)
[11] Manohar S, Kharine A, van Hespen J C G, Steenbergen W and van Leeuwen T G 2005 *Phys. Med. Biol.* **50** 2543
[12] Andreev V G, Karabutov A A and Oraevsky A A 2003 *IEEE. T. Ultrason. Ferr.* **50** 1383
[13] Zhang H F, Maslov K, Sivaramakrishnan M, Stoica G and Wang L H V 2007 *Appl. Phys. Lett.* **90** 053901
[14] Li M L, Oh J T, Xie X Y, Ku G, Wang W, Li C, Lungu G, Stoica G and Wang L V 2008 *Proc. IEEE* **96** 481
[15] Li C H, Aguirre A, Gamelin J, Maurudis A, Zhu Q and Wang L V 2010 *J. Biomed. Opt.* **15** 010509
[16] Xu M H and Wang L H V 2002 *IEEE Trans. Med. Imaging* **21** 814
[17] Wu D, Tao C, Liu X J and Wang X D 2012 *Chin. Phys. B* **21** 014301
[18] Tao C and Liu X J 2010 *Opt. Express* **18** 2760
[19] Wu D, Tao C and Liu X J 2010 *Acta Phys. Sin.* **59** 5845 (in Chinese)
[20] Xu Y, Wang L V, Ambartsoumian G and Kuchment P 2004 *Med. Phys.* **31** 724
[21] Paltauf G, Nuster R, Haltmeier M and Burgholzer P 2007 *Inverse Probl.* **23** S81
[22] Wu D, Wang X, Tao C and Liu X J 2011 *Appl. Phys. Lett.* **99** 244102
[23] Xu M H and Wang L H V 2005 *Phys. Rev. E* **71** 016706
[24] Wu D, Tao C and Liu X J 2011 *J. Appl. Phys.* **109** 084702